IEEE Access
Multidisciplinary | Rapid Review | Open Access Journal

Received July 18, 2019, accepted August 1, 2019, date of publication August 12, 2019, date of current version August 27, 2019.

Digital Object Identifier 10.1109/ACCESS.2019.2934892

A Dual-Band MIMO Antenna With Enhanced Isolation for 5G Smartphone Applications

WEN JIANG, (Member, IEEE), YANGQIANG CUI, BO LIU, WEI HU, (Member, IEEE), AND YAN XI

National Key Laboratory of Antennas and Microwave Technology, Xidian University, Xi'an 710071, China

Corresponding author: Wen Jiang (jw13@vip.qq.com)

This work was supported by ZTE Industry-Academia-Research Cooperation Funds.

ABSTRACT In this paper, a compact dual-band MIMO antenna array for 5G smartphone applications is proposed. The MIMO antenna consists of eight folded monopole antennas operating at 3.45-GHz band (3300∼3600MHz). And the antenna elements with a size of $6.8 \times 6.6 \times 4$ mm^3 (about $0.078\lambda \times 0.075\lambda \times 0.046\lambda$ at 3.45 GHz), are disposed along each edge of the system circuit board. By introducing the decoupling structures, the isolation between inner antenna elements is improved from 10dB to 15.1dB in 3.45-GHz band (3300∼3600MHz). Meanwhile the inner antenna units can generate an additional operating band covering 2400∼2700MHz due to the coupling effect between the antenna elements and the proposed decoupling structures, which is promising for solving the problem of terminal space shortage. To verify the design principle of the proposed MIMO antenna array, the antenna is fabricated and measured. The measured results of efficiency and ECC are analyzed as well to demonstrate the performance of the proposed MIMO array. Channel capacity, user proximity and SAR analysis and are also given in this paper.

INDEX TERMS Decoupling structure, eight-element array, high isolation, MIMO antenna.

I. INTRODUCTION

The fifth-generation (5G) communication technology can provide many advantages such as higher transmission rate and shorter latency over the current 4G system. It has been demonstrated that to achieve higher transmission rate for the 5G operation below 6 GHz. Multiple-input and multiple-output (MIMO) technology has been used to significantly increase the channel capacities of wireless communication systems. The more antenna elements set in MIMO array, the higher channel capacities will be achieved. However, due to the limited space in mobile smartphone, it has been a challenge to design a compact multi-element MIMO antenna array with high isolations for the 5G mobile communication systems [1], [2].

Recently, in order to meet the needs of high rate and large capacity of data transmission, various MIMO antenna arrays and decoupling structures are proposed and studied, such as self-isolated technology [3], parasitic structures and polarization diversity technology [4], Orthogonal-mode isolation technology [5], neutralization line technology [8] and so on [9]–[14]. The detailed comparisons of these decoupling technologies are listed in table 1. We notice that the size of MIMO elements should be reduced as much as possible and MIMO array should be properly decoupled according to the form of element and arrangement to achieve better performance form the table.

At present, with the development of wireless technology, the available area for antennas in the terminal mobile phone is continuously reduced, and the research on reducing the antenna size in the terminal mobile phone has attracted wide attention. In the design of mobile MIMO antennas, many researchers use decoupling structures to reduce the coupling effect between antenna elements and improve the isolations. However, decoupling structure is only used to reduce the coupling effect for terminal antennas limited by spatial size, which seems to be a waste of space. Therefore, we study how to make decoupling structure to implement more functions. If the decoupling structure can also make the antenna change from single frequency to multi-frequency operation, improve the antenna pattern, reduce the SAR value of the antenna, etc., this is far-reaching for antenna design.

In this paper, a compact dual-band eight elements MIMO antenna array with decoupling structure is presented. The innovation of the decoupling structure proposed in this paper not only improves the isolations effectively, but also generates

The associate editor coordinating the review of this article and approving it for publication was Lin Peng.

This work is licensed under a Creative Commons Attribution 4.0 License. For more information, see http://creativecommons.org/licenses/by/4.0/

TABLE 1. Performance comparison with previous published literatures.

Ref.	Decoupling Method	Element size(mm^3)	Decoupling structure size(mm^3)	Total size(mm^3)	Isolation (dB)	ECC	New band from decoupling structure
[3]	Self-isolated	17.4×6×0.8 (single-element)	17.4×6	150×75×6 (eight-element)	>19.6	<0.013	No
[4]	Parasitic structures/ Polarization isolation	30×30×1.6 (dual-element)	16.4×16.4×1.6	150×75×1.6 (eight-element)	>15	<0.01	No
[5]	Orthogonal-mode	12×7×0.8 (single-element)		150×73×7 (eight-element)	>17dB	<0.1	No
[6]	No	17×6×2.8 (single-element)		136×68×2.8 (eight-element)	10dB	<0.2	No
[7]	Hybrid decoupling	12.5×4.9×0.8 (single-element)	20×4.5	124×74×6 (eight-element)	>15dB	<0.15	No
[8]	Neutralized line	15×7×0.8 (single-element)	10x0.2	150×75×6 (eight-element)	>11.5	<0.08	No
[9]	Orthogonal arrangement/ defected ground	21.5×3×0.8 (single-element)		150×80×0.8 (eight-element)	>17.5	<0.05	No
[10]	Pattern diversity	14x39.7x0.8 (single-element)		100x40 (four-element)	>15	<0.15	No
This work	Grounding branch	6.8×6×4 (single-element)	32.3x3.8x0.8	124×74×4 (eight-element)	>15.1	<0.2	Yes

a new resonant point in another frequency band covering 2400 ∼ 2700MHz to achieve a dual-band operating performance, thus it can effectively improve space utilization in mobile devices. By employing the decoupling structure, the isolations between the inner antenna elements (Ant2, Ant3, Ant6, Ant7) are improved from 10dB to 15.1dB in 3.45-GHz band (3300 ∼ 3600MHz). The details of the proposed MIMO antenna array are described, and the results of S-parameters, radiation fields and user effects of MIMO antenna array are also presented.

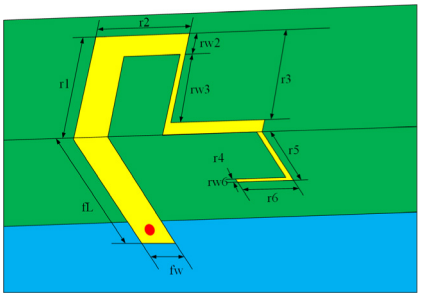

FIGURE 1. Details sizes of MIMO antenna element.

II. ANTENNA ELEMENT AND DECOUPLING

The geometries of the proposed antenna elements and decoupling structure are shown in Figure 2. The antenna elements are placed symmetrically on the top and inner surfaces of the Sub1 (System circuit board) and Sub2 (Side frame), which are respect to the center of the decoupled structure on the top surfaces of Sub1. The side-edge frame with a size of $74\times5mm^2$ and the system circuit board with an overall size of $124\times74mm^2$ are fabricated using FR4 substrate with a thickness of 0.8mm, and a relative dielectric constant of 4.4 and a loss tangent of 0.02.

A. ANTENNA ELEMENT

The element of the MIMO antenna array realizes the design of larger effective length in smaller space by bending the monopole antenna and printing it on the Sub 1 and the Sub 2, which results in a very significant reduction in the antenna size. The antenna element only occupies an area of 6.8 × 6.6× 4mm ^{3}, which contributes to improve the isolations of antenna elements because of the larger distances between the adjacent elements. Ant1-2 and Ant3-4 are symmetric about the decoupling structure, and the same as Ant 5-8.

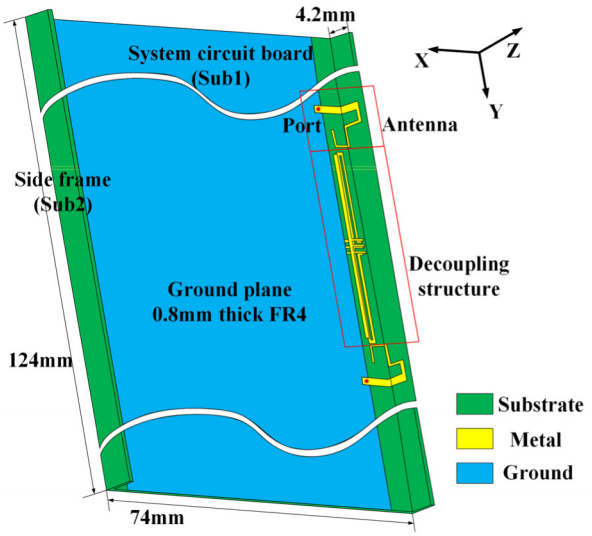

FIGURE 2. Geometries of MIMO antenna elements and decoupling structure.

TABLE 2. Evolution of unit design.

Model	Model structure	Size(mm^3)	Operating band (GHz)
(1)	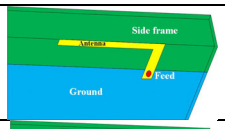	13.6*6.6*0	3.06-3.92
(2)	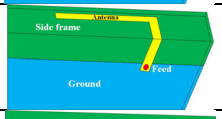	12.5*6.6*4	3.0-4.15
(3)	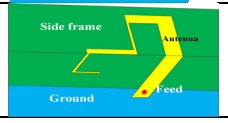	6.8*6.6*4	3.14-3.71

Monopole antenna is a common terminal antenna type, which has the characteristics of easy to manufacture. As we can see in Table 2, by bending the radiated strip, the final model size decreases by 50%. The impedance bandwidth of the antenna is 3.14-3.71 GHz. In MIMO array, the bandwidth of MIMO antenna is narrowed due to the influence of adjacent antennas. But it still covers the sub-6G band (3300-3600MHz).

B. DECOUPLING STRUCTURE

As the mutual coupling between the antenna elements deteriorates the channel capacities of MIMO antenna system, decoupling structures are utilized between the antenna elements to enhance isolations. Common decoupling structure includes grounded branch, neutralization lines, decoupling networks and so on. These decoupling structures have been studied and widely used to reduce the coupling effect of MIMO antenna arrays.

The decoupling structure designed in this paper works like a grounded branch. By absorbing the energy coupled from the adjacent antenna, the coupling effect on the other antenna unit is reduced. The decoupling structure is shown in Figure 4. The size of decoupling structure is 32.3 mm × 3.36 mm (about 0.371λ× 0.038λ at 3.45 GHz).

FIGURE 3. Geometry of decoupling structure.

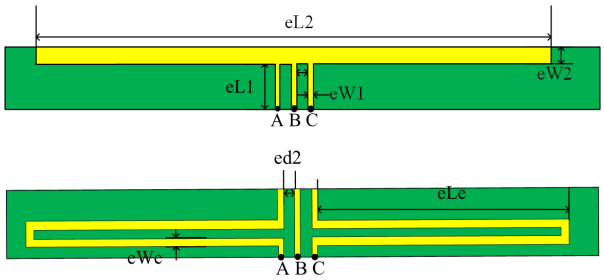

FIGURE 4. Geometry of decoupling structure.

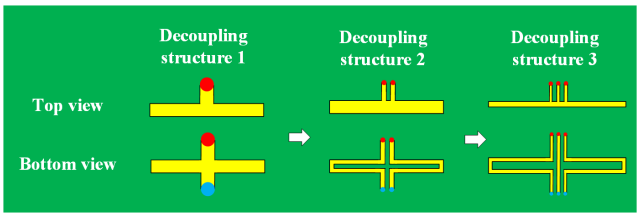

FIGURE 5. Geometry of decoupling structure (top view, bottom view).

The proposed decoupling structure consists of multiple strips printed on both sides of the Sub1, which are connected by short strips with three points A, B and C. Wherein, the strip from top view is connected by thin metal strips through three thin strips to three points A, B, and C. The strips from bottom view is composed of three structurally symmetrical metal strips, and one end of the metal strips are connected to the floor, while the other end of the metal strips are connected to points (A, B, C) in turn.

Figure 5 shows the evolution process of the decoupling structure proposed in this paper. At first, the floor branch is set on the defective ground. Then, rectangular metal patches are set on the dielectric plates of two MIMO antenna elements through the truncated lines of the floor. Finally, the final model structure is obtained by further optimization design of the structure. In this figure, the red dot represents the position of the stub connecting the upper and lower decoupling metal patches, and the blue dot represents the point of the ground plane.

From Figure 6, with the continuous improvement of decoupling structure, the coupling effect between MIMO antenna elements is getting lower and lower, and the isolation effect between them is improved at 3.45-GHz band (3300∼3600MHz).

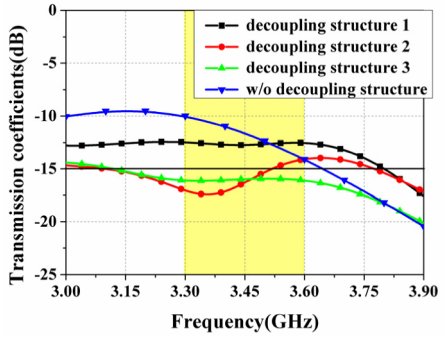

FIGURE 6. Simulated transmission coefficients of different structures.

TABLE 3. Parameters of the MIMO antenna.

Parameters	Wg	Wd	fL	fW	r1	r2
Dimension (mm)	66	4	6.6	1.2	4	2
Parameters	r3	r4	r5	r6	rw2	rw3
Dimension (mm)	3	3.6	3	2.8	0.8	0.2
Parameters	rw6	eW1	eL1	eW2	eL2	ed
Dimension (mm)	0.2	0.3	2.8	3	31	0.7
Parameters	eLe	eWe	ed2			
Dimension (mm)	15	0.5	0.7			

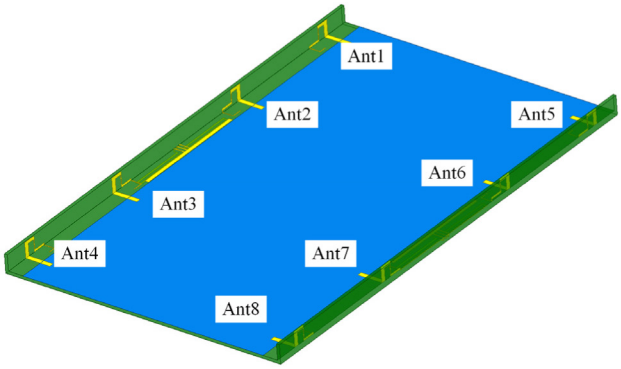

FIGURE 7. Configuration of the eight-antenna MIMO array.

Similar to the working principle of grounding branch, this decoupling structure can absorb most of the coupling energy generated by adjacent MIMO antenna elements. Therefore, the proposed decoupling structure reduces the coupling effect between antennas, and the isolation is improved from 10dB to 15.1dB in 3.45-GHz band (3300∼3600MHz). Meanwhile, it also generates an additional resonant point in 2.55GHz band (2400∼2700MHz) for the inner antennas (Ant 2, Ant 3, Ant 6, Ant 7). The size of the decoupling structure is 32.3 × 3.36mm^2, which consists of multiple strips printed on both sides of the Sub1 connected through metal patches printed on the side-edge frame. The detail geometry of the MIMO antenna array is listed in Table 3 and the configuration of the eight-antenna MIMO array is shown in Figure 7.

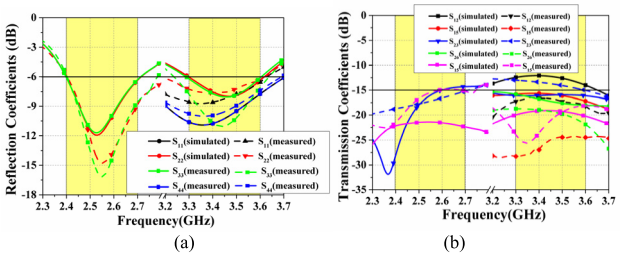

FIGURE 8. Simulated and measured (a) reflection coefficients and (b) transmission coefficients.

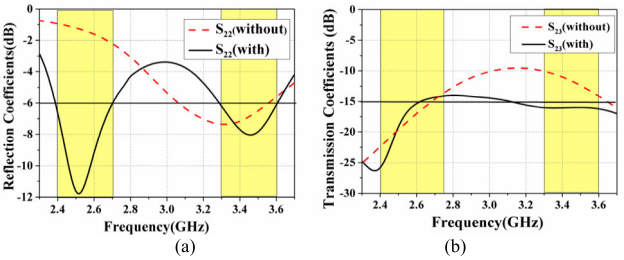

FIGURE 9. Comparison of (a) reflection coefficients and (b) transmission coefficients of MIMO antenna with/without decoupling structure.

C. REASULTS ANALYSIS

The simulated and measured results of S-parameter and far field characteristics of MIMO antenna array are shown in Figure 8, which are obtained with the help of the HFSS version 19.0 software. The simulated and measured results of the proposed MIMO antenna are in good agreement.

The 6-dB impedance bandwidth of Ant2, Ant3 are 2400-2700MHz and 3300-3600MHz, and that of Ant1, Ant4 are 3050-3700MHz. The measured results of Ant2, Ant3 are better than the simulation results at high frequencies, shown in Figure 8(a). Because of Ant1, Ant 4, Ant 5, Ant 8 is in the non-resonant state at low frequencies, the coupling effects between these antenna elements are not considered at low frequencies. Figure 8(b) shows the simulated and measured results of transmission coefficients of the proposed MIMO antenna array.

From Figure 9, before the decoupling structure is loaded, Ant2 works in a single frequency band the isolation between Ant2 and Ant3 is lower than 10dB in 3.45GHz band without the decoupling structure, and the coupling between Ant2 and Ant3 is serious. By introducing the decoupling structure between Ant2 and Ant 3, the isolation between Ant2 and Ant3 is improved from 10 dB to 15.1dB in the 3.45GHz band, and Ant2 achieves dual-frequency operation characteristics. It is the same for Ant 3, Ant 6 and Ant 7 due to the antenna symmetrical structure.

TARC is an imperative parameter to judge the MIMO antenna performance. TARC is calculated by S parameters of MIMO ports. TARC is the ratio of square root of total reflected power to the total incident power.

$$\Gamma_a^t = \frac{\sqrt{p_a - p_r}}{p_a} \tag{1}$$

where p_a denotes incident power and p_r denotes radiation power for MIMO antenna system.

For a lossless antenna, the TARC can be calculated using $[S_P]$. For a given excitation $[a]$ [15]

$$\Gamma_a^t = \frac{\sqrt{\sum_N^{i=1} |b|^2}}{\sqrt{\sum_N^{i=1} |a|^2}} \tag{2}$$

where

$$[b] = [S_p] \cdot [a] \tag{3}$$

We do not need to define the TARC as a complex number since the phase reference plane does not have any physical meaning for a multiport antenna. The TARC is a real number between zero and one. When the value of the TARC is equal to zero, all the delivered power is radiated and when it is equal to one, all the power is either reflected back or goes to the other ports. None of the former parameters like ARC or the scattering matrix can show this for the general case [16].

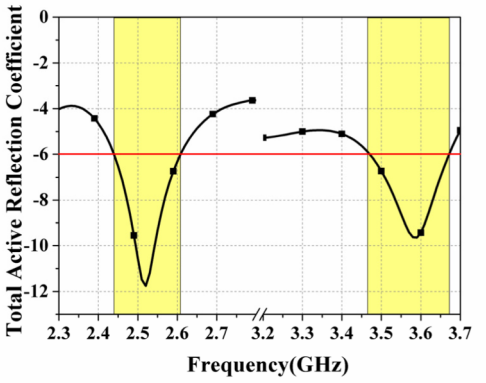

FIGURE 10. TARC curve of the proposed MIMO antenna.

From Figure 10, we can see that the – 6-dB bandwidth of TARC reflection coefficient is 2.44-2.63 GHz and 3.46-3.67 GHz, which has the same trend as S parameter reflection coefficient.

From the surface current distribution in decoupling structure of Figure 11 (a) and (b), the coupling energy from Ant2 to Ant3 is absorbed by the decoupling structure. After adding decoupling structure, the maximum current amplitude of adjacent elements at the same time decreases by more than 50%, which shows that the structure effectively reduces the coupling effect of antenna, so that the isolation can be improved effectively.

For the coupling effect between Ant1 and Ant2, the distance between Ant2 and Ant3 can be reduced by reducing the size of the decoupling structure proposed in this paper. At the same time, the distance between Ant 1 and Ant 2 can be increased, and the isolation can be improved.

Because the structure of MIMO antenna array is symmetrical, only the patterns of Ant 1 and Ant 2 are given, as shown in Figure 12. Meanwhile, the radiation pattern of Ant 1 is only given at 3.45 GHz (the operating frequency band of Ant1 is

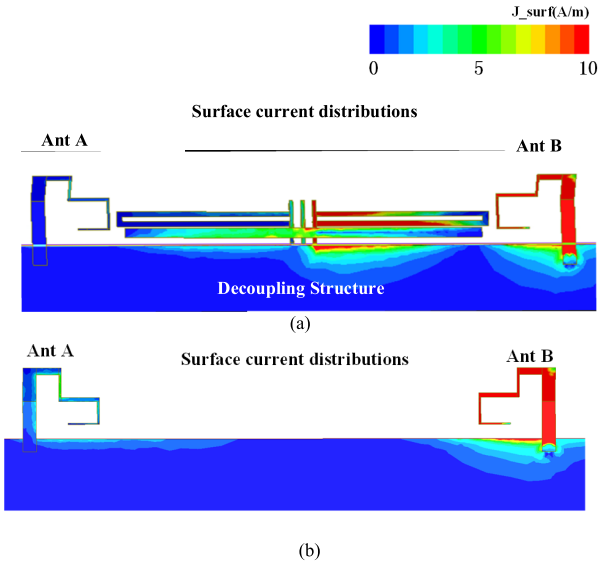

FIGURE 11. Simulated surface current distributions of the antenna (a) with decoupling structure (b) without decoupling structure.

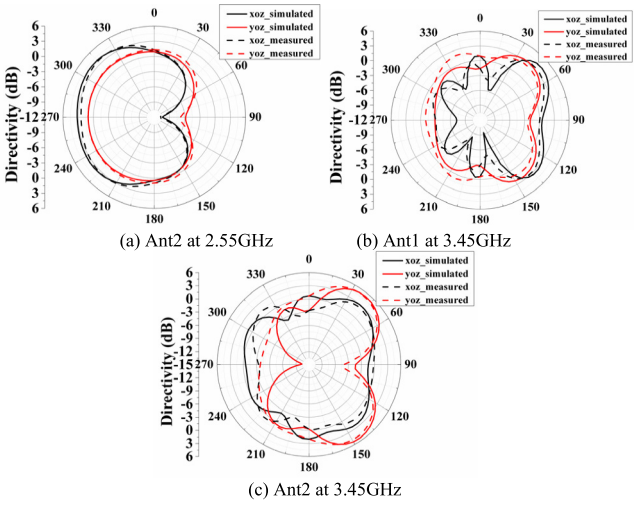

FIGURE 12. Radiation pattern of the proposed antenna.

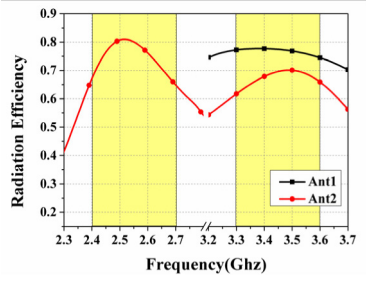

FIGURE 13. Simulated antenna radiation efficiency.

3300-3600 MHz). From the figure, it can be seen that there is good consistency with pattern between Ant 1 and Ant 2 at the same frequency point.

The radiation efficiency of each MIMO antenna elements in the operating frequency band is greater than 0.6, as shown in Figure 13. Since the low frequency is not the

operating band for the Ant 1, the result is not shown in this figure.

III. MIMO ANTENNA ARRAY CHANNEL CAPACITY

With the development of wireless communication systems, the utilization of channel resources is more extensive and thorough, which required that we should understand the characters of wireless channel, make a comprehensive and accurate description of these resources through the establishment of channel models. The system of multiple input multiple output (MIMO) adopted multi-antenna both in transmitter and receiver, which not only enhances the performance of the system, but also improves the channel capacity compared with single input single output systems. Channel capacity is one of important parameters of MIMO antenna system.

ECC (envelope correlation coefficient) is an important parameter of MIMO antenna array. Theoretically, the smaller the value is, the better the MIMO performance is. However, too much pursuit of the minimum value of ECC will sacrifice other performance of MIMO antenna, such as antenna radiation efficiency. Therefore, in practical antenna design, the value of ECC should not be greater than 0.2 in operating bands.

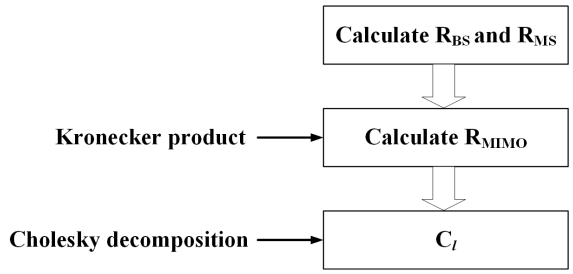

FIGURE 14. Flow chart for calculating matrix C_l.

Figure 14 shows the calculated envelope correlation coefficients of MIMO antenna elements. The obtained envelope correlation coefficient (ECC) of the working antennas (Ant2, Ant3) is less than 0.21 in 2.55GHz band and 3.45GHz band, which shows good performance for mobile terminals communication.

Theoretically, the capacity of the MIMO system grows linearly with the number of antennas. However, the correlation in the MIMO channel induces a loss of capacity. The correlation coefficients of MIMO antenna array are shown in Figure 15. In the case of high SNR, capacity loss can be derived from (6), and the result is shown in Figure 15.

$$C_{(loss)} = -log_2 det(\psi^R) \tag{4}$$

where ψ^R are a 4×4 correlation matrix at 2400-2700MHz, and an 8×8 correlation matrix at 3300-3600MHz respectively. The matrix elements can be calculated by,

$$|\rho|^2 \approx \rho_e \tag{5}$$

For the capacity loss of antenna arrays, we mainly focus on the frequency range near and at the resonance frequency.

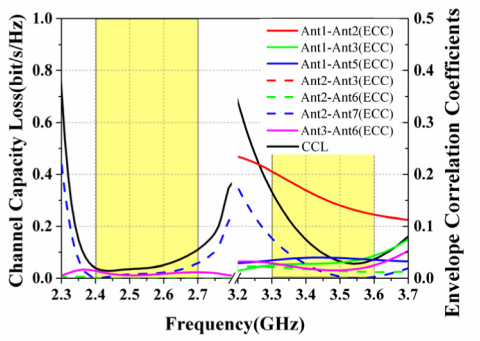

FIGURE 15. Simulated envelope correlation coefficients and CCL.

TABLE 4. Assessment of the proposed antenna with the other published antenna.

	Size of the antenna	Impedance Bandwidth	CCL (bit/s/Hz)	ECC
This work	124*74*4mm^3 (eight units)	2.4-2.7GHz 3.3-3.6GHz (-6dB)	<0.32	<0.21
[17]	36*18mm^2 (four units)	3.2-12GHz (-10dB)	<0.8	<0.008
[15]	55*49*1.6mm^3 (two units)	8-12GHz (<-20dB)	<0.26	<0.016
[18]	50*30mm^2 (two units)	3.1-9.7GHz (-10dB)	<0.2	<0.12

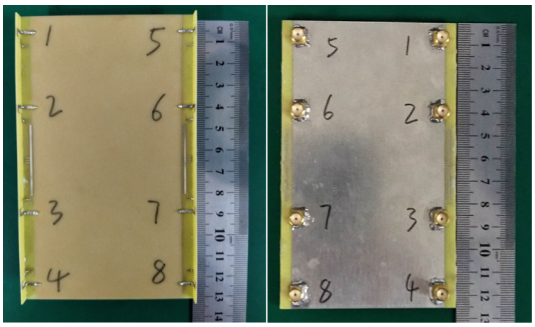

FIGURE 16. Fabricated prototype of the MIMO antenna.

The capacity loss has the same tendency as ECCs. As shown in Figure 14, the curves show the lowest loss of capacity at 2.44GHz and 3.54GHz in high and low frequency bands, respectively, because it has the lowest envelope correlation coefficient. We can infer the effect of correlation between antennas on channel capacity by Figure 14.

The channel capacity loss parameter guarantees the good MIMO performance of the MIMO antenna with proposed decoupling structure.

The channel capacity of the MIMO antenna proposed in this paper is calculated based on the correlation method model.

Assume that the receiving and transmitting antennas are eight-element MIMO antennas in this paper. Matrix $\boldsymbol{C_l}$ is calculated firstly, which is shown in figure 16. $\boldsymbol{H}$ matrix can be obtained by reshaping of $\boldsymbol{H_v}$ vector, and matrix $\mathbf{R}$ is obtained from formula (2). Then the channel capacity value is obtained from formula (3).

Due to the lower ECC value of MIMO antenna, the arithmetic square root of the envelope correlation coefficient is taken as the corresponding elements of matrix $\mathbf{R_{MS}}$ and matrix $\mathbf{R_{BS}}$. The matrix $\mathbf{R_{MIMO}}$ is obtained by Kronecker product of the two matrices, and the matrix $\mathbf{C_l}$ is obtained by Cholesky decomposition.

$$H_v = \sqrt{P_L} Ca \tag{6}$$

P_L is the power on a single link. In the formula (1), $\boldsymbol{a}$ means the zero-mean complex Gaussian distribution and it's independent of each other.

$$R = HH^H \tag{7}$$

$$C = \sum_{k=1}^{K} \log_2 det(I + \frac{\lambda_k}{K}\frac{P}{\sigma^2}) = \log_2 det(I + R\frac{P}{K\sigma^2}) \tag{8}$$

$\boldsymbol{I}$ is the unit matrix, $\boldsymbol{R} = \boldsymbol{HH}^H$, K is the rank of matrix $\boldsymbol{R}$, P is the total power and $\sigma 2$ is the noise power. The channel capacity of the 8-element MIMO antenna array proposed in this paper is about 35 bps/Hz by assuming that the channel obeys Rayleigh fading condition and the signal-to-noise ratio is 20dB in the identically and independently distributed propagation condition. The code is written by MATLAB simulation software, and the final result is obtained [19].

IV. USER PROXIMITY ANALYSIS AND SAR ANALYSIS

A. USER PROXIMITY ANALYSIS

With the development of wireless communication technology, the demand for mobile terminal antenna is also constantly upgrading. People concern the influence of the user proximity on the mobile phone antenna. The mobile phone environment and user proximity setup are created in numerical simulation software HFSS 19.0. All the simulation setups are created to be more realistic. There are three common ways to place smartphones, including holding a phone in one hand, browsing information in one hand and playing games in both hands. Then, aiming at these three specific antenna placement modes, combined with the corresponding human body tissues, this paper discusses the impact of human body on mobile MIMO antenna in these situations.

By analyzing the antenna radiation characteristics, the lobes with stronger antenna gain deviate from the tissues and organs of the human body in the second mode (data mode). Therefore, the electromagnetic energy absorbed by the human body is low, and the radiation efficiency of antenna in this mode is less affected.

The specific placement modes of mobile phone are shown in Figure 17, and the simulated results of S-parameters and radiation efficiency are shown in Figure 18, 19 and 20. Compared with the antenna performance when the human tissue model is not involved, we can find that the antenna performance has changed slightly, which is caused by the large distance between MIMO antenna elements and human tissues such as fingers, mainly reflected in the radiation efficiency and impedance matching of the antenna. The radiation efficiency of the antenna decreases and the impedance matching

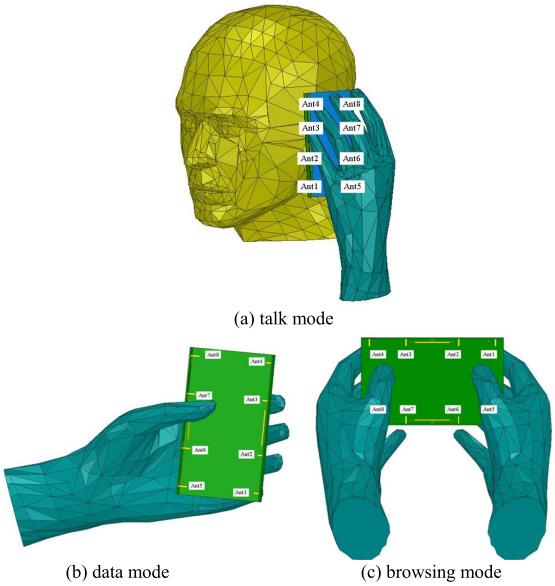

(a) talk mode

(b) data mode (c) browsing mode

FIGURE 17. Three kinds of user proximity.

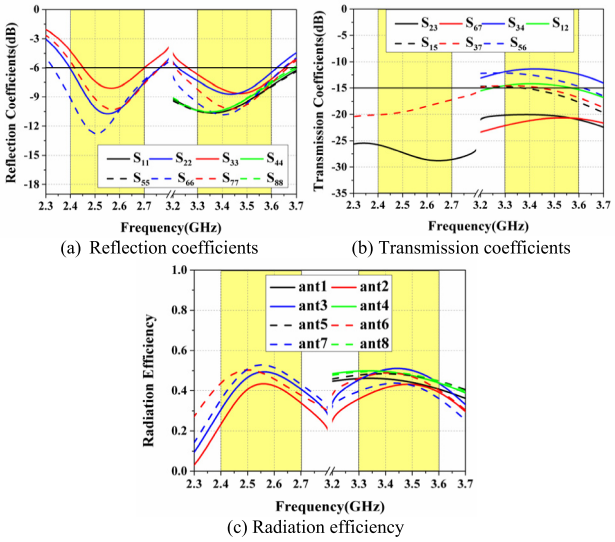

(a) Reflection coefficients (b) Transmission coefficients

(c) Radiation efficiency

FIGURE 18. Performance of the proposed MIMO antenna at talk mode.

of the antenna become worse. Among these three modes, the data mode has the lowest impact on the antenna, because in this mode, the distance between human tissue and MIMO antenna elements is farther than the other two modes.

B. SAR ANALYSIS

SAR (Specific Absorption Rate) characterizes the impact of electromagnetic radiation on human body. The meaning of SAR is the electromagnetic power absorbed or consumed per unit mass of human tissues in unit time, in W/kg or mW/g. It has different standards for SAR in the United States and Europe, the usage of the United States is 1g standard, and the usage of Europe is 10g standard. SAR is divided into local SAR and average SAR. SAR has become a compulsory index to evaluate mobile communication terminals.

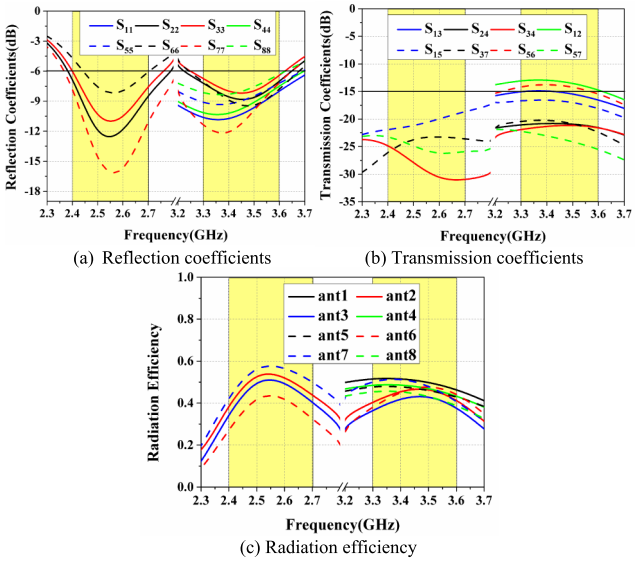

(a) Reflection coefficients (b) Transmission coefficients

(c) Radiation efficiency

FIGURE 19. Performance of the proposed MIMO antenna at data mode.

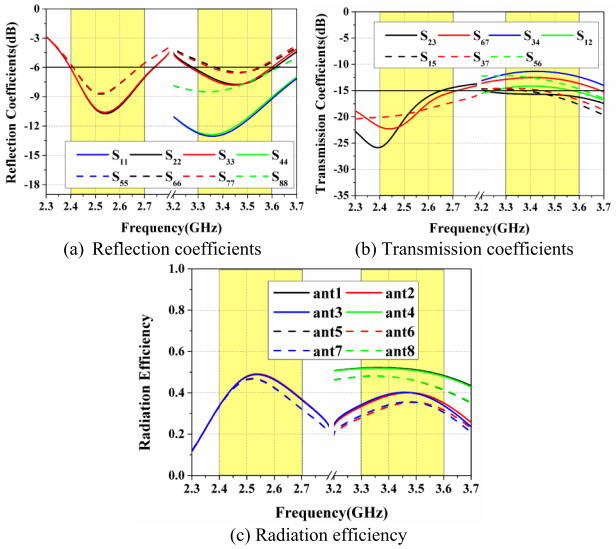

(a) Reflection coefficients (b) Transmission coefficients

(c) Radiation efficiency

FIGURE 20. Performance of the proposed MIMO antenna at browsing mode.

The specific absorption rate (SAR) is usually used as an indicator of electromagnetic radiation in the study of microwave biological. The SAR caused by the human exposure to radiofrequency electromagnetic fields [20], it is defined as the electromagnetic radiation energy absorbed or consumed by the unit mass tissue in the human body. The formula for calculating specific absorption rate is as follows:

$$\mathrm{SAR} = \frac{d}{dt}\left(\frac{\mathrm{dW}}{dm}\right)\frac{d}{dt}\left(\frac{\mathrm{dW}}{\rho dv}\right) \tag{9}$$

In the actual calculation or measurement, the radiation power is not easy to obtain, therefore, the (1) can be deformed as

$$\mathrm{SAR} = \frac{\sigma E^2}{\rho} \tag{10}$$

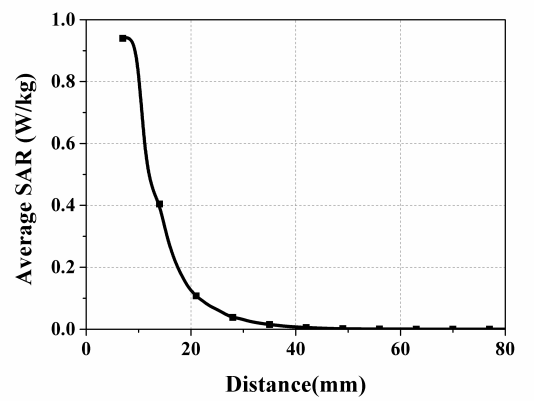

FIGURE 21. Average SAR values distribution at talk mode.

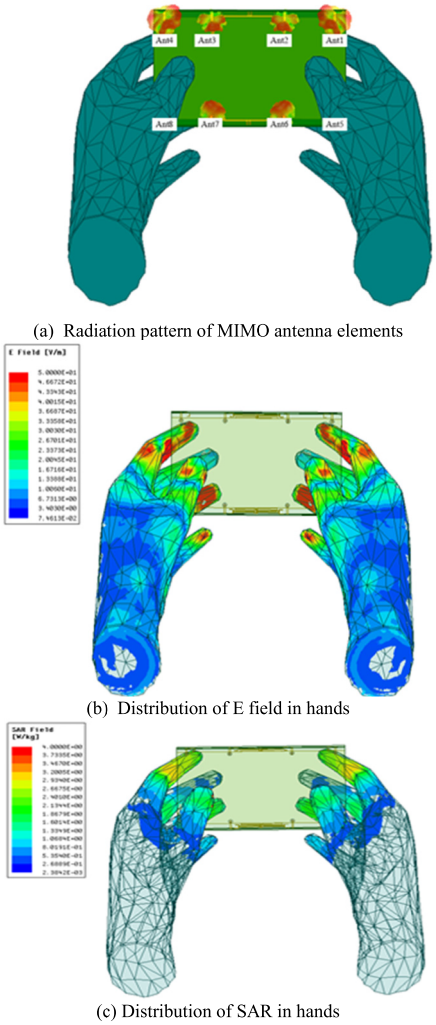

(a) Radiation pattern of MIMO antenna elements

(b) Distribution of E field in hands

(c) Distribution of SAR in hands

FIGURE 22. Analysis of MIMO antenna SAR at browsing mode (3.45GHz).

where σ and ρ represent the electric conductivity (S/m) and mass density (kg/m^3) of the medium, respectively. The density and electrical conductivity are known, so that if we know the electric field intensity (E^2), the value of SAR will be calculated. The lower of SAR value, the amount of radiation absorbed by the human is less.

TABLE 5. Assessment of the proposed antenna with the other published antenna.

	Radiation efficiency (%)		Peak SAR value(W/kg)	
	2.55GHz	3.45GHz	2.55 GHz	3.45 GHz
Mode 1	Ant2: 43 Ant3: 49 Ant6: 48 Ant7: 53	Ant1: 45 Ant5: 48 Ant2: 44 Ant6: 48 Ant3: 51 Ant7: 43 Ant4: 48 Ant8: 49	0.90	0.80
Mode 2	Ant2: 54 Ant3: 51 Ant6: 44 Ant7: 58	Ant1: 51 Ant5: 47 Ant2: 47 Ant6: 47 Ant3: 43 Ant7: 50 Ant4: 48 Ant8: 44	0.67	1.09
Mode 3	Ant2: 50 Ant3: 50 Ant6: 46 Ant7: 46	Ant1: 52 Ant5: 47 Ant2: 39 Ant6: 35 Ant3: 40 Ant7: 35 Ant4: 51 Ant8: 47	1.18	0.65

According to simulation software and the human tissue model HFSS software, we simulated the SAR value of three different handheld modes, and the corresponding analysis is given as follow [21].

In the definition of SAR value, we can see that the factor that affects SAR value related to antenna is $\boldsymbol{E}$. According to antenna theory, the electric field will decrease with the increase of distance. Electric field is the only factor of the antenna affecting the SAR value, and the distance between antenna and body issue is very sensitive to SAR value. As can be seen in Figure 21, the MIMO antenna is with an accepted power of $P_{\text{total}} = 20\text{dBm}$ (100mW), and each element is allowed to transmit at most $P_{\text{unit}} = 14\text{dBm}$ (25mW). The 1g issue average SAR value shows a steep decline trend in a certain distance.

More results will be omitted here due to limited space of this letter. From the Figure 22, it can be seen that the SAR value distribution near the finger of the antenna is higher, and the SAR value decreases obviously with the increase of the distance. The same result can be obtained from the pattern analysis of MIMO antenna.

In order to fit the actual situation and the environment when handheld mobile phone antenna, the distance between antenna and human tissue is less than 5 mm, which is the main reason for the higher SAR value. Because of this distance, the SAR values change dramatically and sensitively.

Reducing SAR value of mobile phone antenna will also be the work we will continue to do in future.

V. CONCLUSION

A compact dual-band MIMO antenna array has been proposed. The MIMO antenna consists of 8 folded monopole antennas operating at 3.45-GHz band (3300∼3600MHz). And the antenna elements with a size of 6.8 × 6.6 mm2 are disposed along each edge of the system circuit board. By introducing the decoupling structures, the isolation between inner antenna elements is improved from 10dB to 15.1dB in 3.45-GHz band (3300∼3600MHz). Meanwhile the inner antenna units can generate an additional operating band covering 2400∼2700MHz due to the coupling effect between the antenna elements and the proposed decoupling structures, which is promising for solving the problem of terminal space shortage. The measured results of efficiency and ECC are analyzed as well to demonstrate the performance of the proposed MIMO array. The performance of the proposed antenna with user proximity is acceptable for practical application. The way of improving antenna space utilization provides a new idea and direction for the design of dual-frequency terminal MIMO antenna.

REFERENCES

[1] S. Q. Li, "5G: Intelligent mobile communication 1.0," *ZTE Technol.*, vol. 22, no. 3, pp. 47–48, Jun. 2016.
[2] L. Hongjia, C. Xin, and Z. Xu, "Cooperative management architecture and mechanism of 55 G-oriented distributed mobile cloud computing G-oriented," *ZTE Commun.*, vol. 21, no. 2, pp. 14–19, Apr. 2014.
[3] A. Zhao and Z. Ren, "Size reduction of self-isolated MIMO antenna system for 5G mobile phone applications," *IEEE Antennas Wireless Propag. Lett.*, vol. 18, no. 1, pp. 152–156, Jan. 2019.
[4] N. O. Parchin, Y. I. A. Al-Yasir, A. H. Ali, I. Elfergani, J. M. Noras, J. Rodriguez, and R. A. Abd-Alhameed, "Eight-element dual-polarized MIMO slot antenna system for 5G smartphone applications," *IEEE Access*, vol. 7, pp. 15612–15622, 2019.
[5] L. Sun, H. Feng, Y. Li, and Z. Zhang, "Compact 5G MIMO mobile phone antennas with tightly arranged orthogonal-mode pairs," *IEEE Trans. Antennas Propag.*, vol. 66, no. 11, pp. 6364–6369, Nov. 2018.
[6] D. Q. Liu, M. Zhang, H. J. Luo, H. L. Wen, and J. Wang, "Dual-band platform-free PIFA for 5G MIMO application of mobile devices," *IEEE Trans. Antennas Propag.*, vol. 66, no. 11, pp. 6328–6333, Nov. 2018.
[7] W. Jiang, B. Liu, Y. Cui, and W. Hu, "High-isolation eight-element MIMO array for 5G smartphone applications," *IEEE Access*, vol. 7, pp. 34104–34112, 2019.
[8] J. L. Guo, L. Cui, C. Li, and B. H. Sun, "Side-edge frame printed eight-port dual-band antenna array for 5G smartphone applications," *IEEE Trans. Antennas Propag.*, vol. 66, no. 12, pp. 7412–7417, Dec. 2018.
[9] Y. Li, C.-Y.-D. Sim, Y. Luo, and G. Yang, "High-isolation 3.5 GHz eight-antenna MIMO array using balanced open-slot antenna element for 5G smartphones," *IEEE Trans. Antennas Propag.*, vol. 67, no. 6, pp. 3820–3830, Jun. 2019.
[10] C. F. Ding, X. Y. Zhang, C.-D. Xue, and C.-Y.-D. Sim, "Novel pattern-diversity-based decoupling method and its application to multielement MIMO antenna," *IEEE Trans. Antennas Propag.*, vol. 66, no. 10, pp. 4976–4985, Oct. 2018.
[11] S.-W. Su, C.-T. Lee, and S.-C. Chen, "Very-low-profile, triband, two-antenna system for WLAN notebook computers," *IEEE Antennas Wireless Propag. Lett.*, vol. 17, no. 9, pp. 1626–1629, Sep. 2018.
[12] S. R. Thummaluru, M. Ameen, and R. K. Chaudhary, "Four-port MIMO cognitive radio system for mid-band 5G applications," *IEEE Trans. Antennas Propag.*, to be published.
[13] A. Zhao and Z. Ren, "Wideband MIMO antenna systems based on coupled-loop antenna for 5G N77/N78/N79 applications in mobile terminals," *IEEE Access*, vol. 7, pp. 93761–93771, 2019.

[14] S. R. Thummaluru, R. Kumar, and R. K. Chaudhary, "Isolation and frequency reconfigurable compact MIMO antenna for wireless local area network applications," *IET Microw., Antennas Propag.*, vol. 13, no. 4, pp. 519–525, Mar. 2019.
[15] G. Saxena, P. Jain, and Y. K. Awasthi, "High isolation EBG based MIMO antenna for X-band applications," in *Proc. 6th Int. Conf. Signal Process. Integr. Netw. (SPIN)*, Noida, India, Mar. 2019, pp. 97–100.
[16] S.-W. Su, C.-T. Lee, and F.-S. Chang, "Printed MIMO-antenna system using neutralization-line technique for wireless USB-dongle applications," *IEEE Trans. Antennas Propag.*, vol. 60, no. 2, pp. 456–463, Feb. 2012.
[17] J.-F. Qian, F.-C. Chen, Y.-H. Ding, H.-T. Hu, and Q.-X. Chu, "A wide stopband filtering patch antenna and its application in MIMO system," *IEEE Trans. Antennas Propag.*, vol. 67, no. 1, pp. 654–658, Jan. 2019.
[18] R. Chandel, A. K. Gautam, and K. Rambabu, "Design and packaging of an eye-shaped multiple-input–multiple-output antenna with high isolation for wireless UWB applications," *IEEE Trans. Compon., Packag. Manuf. Technol.*, vol. 8, no. 4, pp. 635–642, Apr. 2018.
[19] S. Zhang, A. A. Glazunov, Z. Ying, and S. He, "Reduction of the envelope correlation coefficient with improved total efficiency for mobile LTE MIMO antenna arrays: Mutual scattering mode," *IEEE Trans. Antennas Propag.*, vol. 61, no. 6, pp. 3280–3291, Jun. 2013.
[20] D. T. Le, L. Hamada, S. Watanabe, and T. Onishi, "A fast estimation technique for evaluating the specific absorption rate of multiple-antenna transmitting devices," *IEEE Trans. Antennas Propag.*, vol. 65, no. 4, pp. 1947–1957, Apr. 2017.
[21] B. Xu, M. Gustafsson, S. Shi, K. Zhao, Z. Ying, and S. He, "Radio frequency exposure compliance of multiple antennas for cellular equipment based on semidefinite relaxation," *IEEE Trans. Electromagn. Compat.*, vol. 61, no. 2, pp. 327–336, Apr. 2019.

WEN JIANG was born in Shandong, China, in November 1985. He received the B.S. and Ph.D. degrees from Xidian University, Xi'an, China, in 2008 and 2012, respectively, where he is currently the Vice Director of the National Key Laboratory of Science and Technology on Antennas and Microwaves and also an Associate Professor. His current research interests include electromagnetic scattering theory and technology, antenna theory and engineering, and electromagnetic measurement theory and technology.

YANGQIANG CUI was born in Shanxi, China, in 1995. He received the B.S. degree in electronic information engineering from Xidian University, Xi'an, China, in 2017, where he is currently pursuing the M.S. degree with the School of Electronics and Communication Engineering. His current research interest includes MIMO antenna theory and design.

BO LIU was born in Shaanxi, China, in 1994. He received the B.S. degree in electromagnetic field and microwave technology from Xidian University, Xi'an, China, in 2017, where he is currently pursuing the M.S. degree. His main research interests include MIMO smartphone antennas and millimeter-wave terminal antennas for 5G mobile communications, as well as multiband smartphone antennas.

WEI HU received the B.S. degree in electronic information engineering and the Ph.D. degree in electromagnetic wave and microwave technology from Xidian University, Xi'an, China, in 2008 and 2013, respectively, where he is currently an Associate Professor with the National Laboratory of Science and Technology on Antennas and Microwaves.

His research interests include multiband and wideband antennas, circularly polarized and dual-polarized antennas, and MIMO technologies.

YAN XI was born in Shaanxi, China, in 1995. He received the B.S. degree in industrial design from Xidian University, Xi'an, China, in 2017, where he is currently pursuing the Ph.D. degree in electromagnetic field and microwave technology with the School of Electronic Engineering. His current research interest includes metasurface and their radiation and scattering applications.